Available online at www.sciencedirect.com

ScienceDirect

Journal of Ocean Engineering and Science 1 (2016) 93–108

www.elsevier.com/locate/joes

A third-order KdV solution for internal solitary waves and its application in the numerical wave tank

Qicheng Meng*, Chongwei Zhang

Department of Mechanical Engineering, University College London, London, UK

Received 26 August 2015; received in revised form 30 October 2015; accepted 30 November 2015
Available online 14 March 2016

Abstract

A third-order KdV solution to the internal solitary wave is derived by a new method based on the weakly nonlinear assumptions in a rigid-lid two-layer system. The solution corrects an error by Mirie and Su (1984). A two-dimensional numerical wave tank has been established with the help of the open source CFD library OpenFOAM and the third-party software waves2Foam. Various analytical solutions, including the first-order to third-order KdV solutions, the eKdV solution and the MCC solution, have been used to initialise the flow fields in the CFD simulations of internal solitary waves. Two groups including 11 numerical cases have been carried out. In the same group, the initial wave amplitudes are the same but the implemented analytical solutions are different. The simulated wave profiles at different moments have been presented. The relative errors in terms of the wave amplitude between the last time step and the initial input have been analysed quantitatively. It is found that the third-order KdV solution results in the most stable internal solitary wave in the numerical wave tank for both small-amplitude and finite-amplitude cases. The finding is significant for the further simulations involving internal solitary waves.

Keywords: Internal solitary waves; Rigid-lid two-layer model; Third-order KdV solution; Numerical wave tank; OpenFOAM; Waves2Foam.

1. Introduction

Internal solitary waves (ISWs) are gravity waves with permanent forms and constant wave speeds that occur within the stratified water body of the ocean. They have been detected in many oceans including the South China Sea [1,28]. They involve giant mass/momentum transportation. The resultant strong water convections and sudden currents could induce unexpected effects on ocean engineering structures and navigating submarines. Thus, a systematic understanding on the generation, propagation and dissipation of the internal solitary waves and eventually wave-wave interactions and their interactions with structures is essential.

At present, investigations on the problems above are mainly based on four methods: satellite remote sensing, field monitoring, laboratory experiments and numerical simulations. The former two methods require a huge cost, while the laboratory experiments are more suitable for specified small projects. It is expected that numerical methods are tending to play more significant roles in recovering the mystery of internal solitary waves.

However, current numerical models for internal solitary waves are still far from mature. Among all the technical difficulties, the accurate generation of internal solitary waves should be one of the priorities. In a numerical wave tank (NWT), the internal solitary waves can be generated through the definition of initial conditions. The initial conditions are determined by different theoretical models that could describe the wave form as well as velocities and pressure within the fluid.

The theoretical models introduced hereinafter are mainly based on the rigid-lid two-layer system. Keulegan [21] had extended the Korteweg–de Vries (KdV) equation to a two-layer system very early. It has been successfully used to explain the internal solitary waves in the Andaman Sea [34]. The theory for internal solitary waves in shallow water is still based on the weakly nonlinear assumptions. Two parameters, denoted

* Corresponding author.
E-mail address: q.meng.12@ucl.ac.uk (Q. Meng).

http://dx.doi.org/10.1016/j.joes.2016.03.002

by ε and β, have to be small. $\varepsilon = a/h'$, where a is the wave amplitude and h' is an intrinsic vertical scale which is taken as the depth of the lower layer in this paper. It can be used to measure the nonlinearity. $\beta = (h/\lambda)^2$, where λ is the characteristic wavelength of the wave. It can be used to measure the dispersion. With the Ursell condition, $\varepsilon = O(\beta) \ll 1$, the KdV equation can be obtained by preserving all the terms in the order of ε in the perturbation expansion of the governing equations based on the potential theory. For convenience, the concept is generalised to the KdV family. The conventional KdV equation is named by the first-order KdV equation. If higher-order terms are included and satisfy both the weakly nonlinear assumptions mentioned above and the Ursell condition, it can be called higher-order KdV equations. The second-order KdV equation has been given by Koop and Butler [22] and Gear and Grimshaw [11]. The third-order KdV solution can be only found in the paper by Mirie and Su [31]. And the same method is used to derive the ninth-order KdV solution later [30]. But no explicit expressions of the ninth-order solution have been given. When the wave amplitude becomes very large and the interface approaches the critical depth, the assumptions and conditions mentioned above will be invalid. Provided ε and β are still small, the nonlinear portion of the equation has to include terms in the orders of both ε and ε^2 to balance the first-order dispersion terms. It results in the extended KdV (eKdV) equation. The solution of the eKdV equation can be found in the papers by Kakutani and Yamasaki [20] and Ostrovsky and Stepanyants [35]. The observations by Stanton and Ostrovsky [39] demonstrated the advantage of the eKdV equation in modelling the highly nonlinear internal solitary waves. The paper given by Choi and Camassa [8] marked establishment of the Miyata–Choi–Camassa (MCC) equations. The model got rid of the restriction of the wave amplitude while the wavelength is still supposed to be long, that is, $\varepsilon = O(1)$ and $\beta \ll 1$. It has been shown that the MCC model is in good agreement with experiments and observations [7,36]. More meticulous experiments have shown that the KdV solution agrees with the experiments the best when the wave amplitude is small; the eKdV solution works the best for the moderate-amplitude internal waves; the MCC model is the most applicable for the large-amplitude internal solitary waves [16].

As introduced above, analytical models are based on many hypotheses, which might show inconsistency in coupling with the general computational fluid dynamics (CFD) codes. From our numerical experiences, we indeed find that adopting above theoretical models as initial conditions does not always lead to stable numerical results.

This research is aimed at simulating more stable internal solitary waves with small or finite amplitude in CFD software by optimising the initial condition. There are two parts. Firstly, we will present a new method to derive the third-order KdV solution based on the weakly nonlinear assumptions. Then various analytical solutions are used to initialise the flow field in a numerical wave tank based on the open source code "Open Field Operation and Manipulation" (OpenFOAM) [42] and the third-party software packages waves2Foam [18].

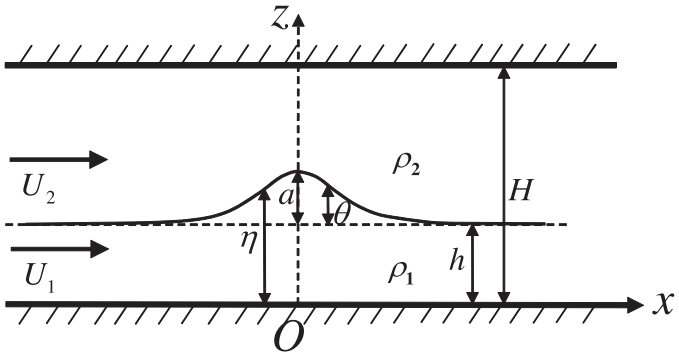

Fig. 1. A rigid-lid two-layer model for the internal solitary wave.

The simulation results will be compared and the best option will be concluded.

2. The third-order weakly nonlinear perturbation solutions

2.1. Mathematical model

Steady two-dimensional potential flow will be considered in this section. The fluid is assumed to be incompressible and inviscid. The flow is irrotational. The two phases of fluid are immiscible. The physical model is a rigid-lid two-layer model. A Cartesian coordinate system moving with the wave peak is defined as in Fig. 1, in which the x-axis lies horizontally and the z-axis is pointing upward. The x-position of the origin is located at the crest or thought. And the z-position of the origin is located at bottom. Consequently, flows come from the infinity at uniform constant speeds U_1 and U_2, respectively, in the two layers. The total depth is H and the depth of the lower layer is h. The displacement of the interface with respect to the bottom is represented by η. For convenience, an ancillary function, $\theta = \eta - h$, is introduced. The amplitude of the wave is donated by a. The subscripts 1 and 2 label the variables of the lower and upper layers, respectively, such as the density ρ, the horizontal fluid velocity u and the vertical fluid velocity w and so on.

For a two-dimensional potential flow, stream functions Ψ_1 and Ψ_2 can be introduced. They are defined as

$$\frac{\partial \Psi_i}{\partial z} = u_i, \quad \frac{\partial \Psi_i}{\partial x} = -w_i, \quad i = 1, 2. \tag{1}$$

They satisfy the Laplace equation, *i.e.*,

$$\Delta \Psi_i = 0, \quad i = 1, 2. \tag{2}$$

The boundary conditions at the upper and lower lids are

$$\Psi_1 = C \ \ on \ \ z = 0; \quad \Psi_2 = U_1 h + U_2(H - h) + C \ \ on \ \ z = H. \tag{3}$$

The constant C can be specified as 0 without loss of generality. The free interface is a streamline and the kinematic condition on it becomes

$$\Psi_1 = \Psi_2 = U_1 h \ \ on \ \ z = \eta(x), \tag{4}$$

The dynamic condition at the interface for the steady flow is

$$\rho_1\left(\frac{1}{2}\left(\frac{\partial\Psi_1}{\partial z}\right)^2+\frac{1}{2}\left(\frac{\partial\Psi_1}{\partial x}\right)^2-\frac{1}{2}U_1^2+g\theta\right)=\rho_2\left(\frac{1}{2}\left(\frac{\partial\Psi_2}{\partial z}\right)^2+\frac{1}{2}\left(\frac{\partial\Psi_2}{\partial x}\right)^2-\frac{1}{2}U_2^2+g\theta\right)\ \text{on}\ z=\eta(x). \tag{5}$$

Eqs. (2)–(5) close the equations for the problem.

Extending the initial ideas put forward by Benjamin and Lighthill [4], six physical parameters are introduced to represent the conservation quantities of the internal solitary wave: the volume flow rate ($Q_i,\ i=1,2$); the energy per unit mass ($R_i,\ i=1,2$); the force plus momentum flux ($S_i,\ i=1,2$) in each layer and the force plus momentum flux over the total depth S. They are defined as

$$Q_1=\int_0^{\eta}u_1dz, \tag{6}$$

$$Q_2=\int_{\eta}^{H}u_2dz, \tag{7}$$

$$R_1=p_1+\rho_1gz+\frac{1}{2}\rho_1\left(u_1^2+w_1^2\right), \tag{8}$$

$$R_2=p_2+\rho_2g(z-H)+\frac{1}{2}\rho_2\left(u_2^2+w_2^2\right), \tag{9}$$

$$S_1=\int_0^{\eta}\left(p_1+\rho_1u_1^2\right)dz, \tag{10}$$

$$S_2=\int_{\eta}^{H}\left(p_2+\rho_2u_2^2\right)dz, \tag{11}$$

$$S=S_1+S_2, \tag{12}$$

where $p_i\ (i=1,2)$ is the corresponding pressure. It can be proved that Q_i, $R_i\ (i=1,2)$ and S are all constants (see Appendix A for the proof for S). Substituting the expressions of p_1 and p_2 obtained from Eqs. (8) and (9) into Eqs. (10) and (11), respectively, we have

$$S_1-R_1\eta+\frac{1}{2}\rho_1g\eta^2=\frac{1}{2}\int_0^{\eta}\rho_1\left(u_1^2-v_1^2\right)dz, \tag{13}$$

$$S_2-R_2(H-\eta)-\frac{1}{2}\rho_2g(\eta-H)^2=\frac{1}{2}\int_{\eta}^{H}\rho_2\left(u_2^2-v_2^2\right)dz \tag{14}$$

The velocities on the flat bottom and top are along the horizontal direction. With the transformation shown in Appendix B, the stream functions Ψ_1 and Ψ_2 can be expanded into Taylor series from $y=0$ and $y=H$, respectively. Those are

$$\Psi_1=zu_1(x,0)-\frac{z^3}{3!}u_1{}''(x,0)+\frac{z^5}{5!}u_1{}^{(4)}(x,0)-\frac{z^7}{7!}u_1{}^{(6)}(x,0)+\frac{z^9}{9!}u_1{}^{(8)}(x,0)-\dots \tag{15}$$

$$\Psi_2=(z-H)u_2(x,H)-\frac{(z-H)^3}{3!}u''_2(x,H)+\frac{(z-H)^5}{5!}u_2^{(4)}(x,H)-\frac{(z-H)^7}{7!}u_2^{(6)}(x,H)+\frac{(z-H)^9}{9!}u_2^{(8)}(x,H)-\dots+Q_1+Q_2 \tag{16}$$

where the primes or the numbers in bracket on superscripts of u denote differentiations with respect to x. Eqs. (15) and (16) give $\Psi_1=0$ at $z=0$, $\Psi_2=Q_1+Q_2$ at $z=H$, respectively. At the interface, where $z=\eta$, $\Psi_1=\Psi_2=Q_1$ satisfying the kinematic interface condition.

Through the stream functions, the horizontal and vertical velocities at any point in both layers can be written as

$$u_1=\frac{\partial\Psi_1}{\partial z}=u_1(x,0)-\frac{z^2}{2!}u''_1(x,0)+\frac{z^4}{4!}u_1^{(4)}(x,0)-\frac{z^6}{6!}u_1^{(6)}(x,0)+\frac{z^8}{8!}u_1^{(8)}(x,0)-\dots, \tag{17}$$

$$w_1=-\frac{\partial\Psi_1}{\partial x}=-zu'_1(x,0)+\frac{z^3}{3!}u_1^{(3)}(x,0)-\frac{z^5}{5!}u_1^{(5)}(x,0)+\frac{z^7}{7!}u_1^{(7)}(x,0)-\frac{z^9}{9!}u_1^{(9)}(x,0)+\dots, \tag{18}$$

$$u_2=\frac{\partial\Psi_2}{\partial z}=u_2(x,H)-\frac{(z-H)^2}{2!}u''_2(x,H)+\frac{(z-H)^4}{4!}u_2^{(4)}(x,H)-\frac{(z-H)^6}{6!}u_2^{(6)}(x,H)+\frac{(z-H)^8}{8!}u_2^{(8)}(x,H)-\dots, \tag{19}$$

$$w_2=-\frac{\partial\Psi_2}{\partial x}=-(z-H)u'_2(x,H)+\frac{(z-H)^3}{3!}u_2^{(3)}(x,H)-\frac{(z-H)^5}{5!}u_2^{(5)}(x,H)+\frac{(z-H)^7}{7!}u_2^{(7)}(x,H)-\frac{(z-H)^9}{9!}u_2^{(9)}(x,H)-\dots. \tag{20}$$

We scale all length dimensions by h, time by h/c_0, where

$$c_0=\sqrt{(g(\rho_1-\rho_2)(H-h)h)/(\rho_2h+\rho_1(H-h))}, \tag{21}$$

and densities by ρ_1. The variables

$$r=\frac{H}{h},\quad \delta=\frac{\rho_2}{\rho_1},\quad \varepsilon=\frac{a}{h}, \tag{22}$$

can be used to simplify the expressions.

We substitute Eqs. (13) and (14) into Eq. (12) and replace the velocity components with stream functions. It yields

$$S-R_1(1+\theta)+\frac{1}{2}(1+\theta)^2-\frac{1}{2}\int_0^{1+\theta}\left(-\frac{1}{2}\Psi_{1x}^2+\frac{1}{2}\Psi_{1y}^2\right)dz-\frac{1}{2}\delta(1-r+\theta)^2-R_2(r-1-\theta)-\frac{1}{2}\delta\int_{1+\theta}^{r}\left(-\frac{1}{2}\Psi_{2x}^2+\frac{1}{2}\Psi_{2y}^2\right)dz=0 \tag{23}$$

which implies the dynamic interface boundary condition. In order to obtain the interface displacement θ in Eq. (23), we have to find a single equation of θ. By defining

$$\xi = \frac{u_1(x,0)}{U_1} - 1, \quad \zeta = \frac{u_2(x,r)}{U_2} - 1, \tag{24}$$

we can rewrite the relationships between the interface displacement and the top or bottom horizontal velocities as:

$$\xi = -\theta - \xi\theta + \frac{\xi''}{3!}(1+\theta)^3 - \frac{\xi^{(4)}}{5!}(1+\theta)^5 + \frac{\xi^{(6)}}{7!}(1+\theta)^7 - \frac{\xi^{(8)}}{9!}(1+\theta)^9 + \cdots, \tag{25}$$

$$\zeta(1-r) = -\theta - \zeta\theta + \frac{\zeta''}{3!}(1-r+\theta)^3 - \frac{\zeta^{(4)}}{5!}(1-r+\theta)^5 + \frac{\zeta^{(6)}}{7!}(1-r+\theta)^7 - \frac{\zeta^{(8)}}{9!}(1-r+\theta)^9 + \cdots. \tag{26}$$

The same assumptions as those used by Long [29] are adopted here. The nth derivatives of θ, ξ and ζ are assumed to have the same order of $\varepsilon^{1+n/2}$. It is another form of the Ursell assumption $U_r = \varepsilon/\beta = O(1)$ as introduced in the introduction. We can use the successive approximation method to solve Eqs. (25) and (26), namely, expressing ξ and ζ by θ. Recalling that θ is a function of x, the magnitude of θ, as x varies, is smaller than that of ε. Thus we can use ε to estimate the truncation errors of the approximations. The solutions of ξ and ζ of lower-order accuracy deduced from Eqs. (25) and (26) are successively iterated into original equations to obtain solutions of higher-order accuracy. The expressions of ξ and ζ with the truncation errors of $O(\varepsilon^6)$ are

$$\begin{aligned}\xi = {} & -\theta + \theta^2 - \theta^3 + \theta^4 - \theta^5 - \frac{\theta''}{6} + \frac{\theta'^2}{3} - \frac{7}{360}\theta^{(4)} - \frac{1}{3}\theta\theta'^2 \\ & + \frac{11}{180}\theta''^2 + \frac{2}{45}\theta'\theta''' - \frac{7}{180}\theta\theta^{(4)} - \frac{31}{15120}\theta^{(6)} \\ & + \frac{1}{3}\theta^2\theta'^2 + \frac{1}{45}\theta'^2\theta'' + \frac{11}{180}\theta\theta''^2 + \frac{2}{45}\theta\theta'\theta''' \\ & + \frac{19}{1260}\theta'''^2 - \frac{7}{360}\theta^2\theta^{(4)} + \frac{47}{3780}\theta''\theta^{(4)} - \frac{11}{1260}\theta'\theta^{(5)} \\ & - \frac{31}{3780}\theta\theta^{(6)} - \frac{127}{604800}\theta^{(8)} + O(\varepsilon^6),\end{aligned} \tag{27}$$

$$\begin{aligned}\zeta = {} & -\frac{\theta}{(1-r)} + \frac{\theta^2}{(1-r)^2} - \frac{\theta^3}{(1-r)^3} + \frac{\theta^4}{(1-r)^4} - \frac{\theta^5}{(1-r)^5} \\ & - \frac{\theta''}{6}(1-r) + \frac{\theta'^2}{3} - \frac{7}{360}\theta^{(4)}(1-r)^3 - \frac{1}{3(1-r)}\theta\theta'^2 \\ & + \frac{11}{180}(1-r)^2\theta''^2 + \frac{2}{45}(1-r)^2\theta'\theta''' - \frac{7}{180}(1-r)^2\theta\theta^{(4)} \\ & - \frac{31}{15120}(1-r)^5\theta^{(6)} + \frac{1}{3(1-r)^2}\theta^2\theta'^2 + \frac{(1-r)}{45}\theta'^2\theta'' \\ & + \frac{11(1-r)}{180}\theta\theta''^2 + \frac{2(1-r)}{45}\theta\theta'\theta''' + \frac{19(1-r)^4}{1260}\theta'''^2 \\ & - \frac{7(1-r)}{360}\theta^2\theta^{(4)} + \frac{47(1-r)^4}{3780}\theta''\theta^{(4)} - \frac{11(1-r)^4}{1260}\theta'\theta^{(5)} \\ & - \frac{31(1-r)^4}{3780}\theta\theta^{(6)} - \frac{127(1-r)^7}{604800}\theta^{(8)} + O(\varepsilon^6).\end{aligned} \tag{28}$$

To verify the derivation, we substitute Eqs. (27) and (28) back to Eq. (24). The $u_1(x,0)$ and $u_2(x,r)$ are expressed by θ consequentially. Then we substitute $u_1(x,0)$ and $u_2(x,r)$ to the stream functions, namely, Eqs. (15) and (16). After sorting out the terms and applying the far field conditions, $Q_1 = U_1$ and $Q_2 = U_2(r-1)$, we have, at the interface where $z = 1+\theta$,

$$\Psi_1 = Q_1 + O(\varepsilon^6), \quad \Psi_2 = Q_1 + O(\varepsilon^6) \tag{29}$$

The streamlines deduced from the two layers coincide at the interface if the terms of $O(\varepsilon^6)$ are neglected. It therefore satisfies the boundary condition at interface to the correct order.

With the expressions above, Eq. (23) is transformed to

$$\begin{aligned}S - {} & R_1(\theta+1) + \frac{1}{2}(\theta+1)^2 - Q_1^2\Big[\frac{1}{2} - \frac{\theta}{2} + \frac{\theta^2}{2} - \frac{\theta^3}{2} \\ & + \frac{\theta^4}{2} - \frac{\theta^5}{2} - \frac{1}{6}\theta'^2 + \frac{1}{6}\theta\theta'^2 + \frac{1}{90}\theta''^2 - \frac{1}{45}\theta'\theta''' - \frac{1}{6}\theta^2\theta'^2 \\ & - \frac{1}{45}\theta'^2\theta'' + \frac{1}{90}\theta\theta''^2 - \frac{1}{45}\theta\theta'\theta''' - \frac{1}{945}\theta'''^2 + \frac{2}{945}\theta''\theta^{(4)} \\ & - \frac{2}{945}\theta'\theta^{(5)}\Big] - \frac{1}{2}\delta(\theta+1-r)^2 - R_2(r-(\theta+1)) \\ & + \delta\left(\frac{Q_2}{r-1}\right)^2\Big[\frac{(1-r)}{2} - \frac{\theta}{2} + \frac{\theta^2}{2(1-r)} - \frac{\theta^3}{2(1-r)^2} \\ & + \frac{\theta^4}{2(1-r)^3} - \frac{\theta^5}{2(1-r)^4} - \frac{1}{6}(1-r)\theta'^2 + \frac{1}{6}\theta\theta'^2 \\ & + \frac{1}{90}(1-r)^3\theta''^2 - \frac{1}{45}(1-r)^3\theta'\theta''' - \frac{1}{6(1-r)}\theta^2\theta'^2 \\ & - \frac{1}{45}(1-r)^2\theta'^2\theta'' + \frac{1}{90}(1-r)^2\theta\theta''^2 - \frac{1}{45}(1-r)^2\theta\theta'\theta''' \\ & - \frac{1}{945}(1-r)^5\theta'''^2 + \frac{2}{945}(1-r)^5\theta''\theta^{(4)} \\ & - \frac{2}{945}(1-r)^5\theta'\theta^{(5)}\Big] = O(\varepsilon^6).\end{aligned} \tag{30}$$

The constants in Eq. (30) are decided by the far field. As there are two superimposed immiscible uniform flows, the values of Q_1, Q_2, R_1, R_2, and S can be given by

$$\begin{cases} Q_1 = U_1, \quad Q_2 = U_2(r-1), \\ R_1 = \frac{1}{2}U_1^2 + 1, \quad R_2 = \frac{1}{2}\delta U_2^2 + \delta(1-r), \\ S = U_1^2 + \frac{1}{2} + \delta U_2^2(r-1) - \frac{1}{2}\delta(r-1)^2. \end{cases} \tag{31}$$

Substitution of Eq. (31) into Eq. (30) gives

$$\begin{aligned} & U_1^2 + \frac{1}{2} + \delta U_2^2(r-1) + \frac{1}{2}\delta(r-1)^2 - \left(\frac{1}{2}U_1^2 + 1\right)(\theta+1) \\ & + \frac{1}{2}(\theta+1)^2 - U_1^2\Big[\frac{1}{2} - \frac{\theta}{2} + \frac{\theta^2}{2} - \frac{\theta^3}{2} + \frac{\theta^4}{2} - \frac{\theta^5}{2} - \frac{1}{6}\theta'^2\end{aligned}$$

$$+\frac{1}{6}\theta\theta'^2+\frac{1}{90}\theta''^2-\frac{1}{45}\theta'\theta'''-\frac{1}{6}\theta^2\theta'^2-\frac{1}{45}\theta'^2\theta''+\frac{1}{90}\theta\theta''^2$$
$$-\frac{1}{45}\theta\theta'\theta'''-\frac{1}{945}\theta'''^2+\frac{2}{945}\theta''\theta^{(4)}-\frac{2}{945}\theta'\theta^{(5)}\Big]$$
$$-\frac{1}{2}\delta(\theta+1-r)^2-\left(\frac{1}{2}\delta U_2^2+\delta g(1-r)\right)(r-(\theta+1))$$
$$+\delta U_2^2\Big[\frac{(1-r)}{2}-\frac{\theta}{2}+\frac{\theta^2}{2(1-r)}-\frac{\theta^3}{2(1-r)^2}$$
$$+\frac{\theta^4}{2(1-r)^3}-\frac{\theta^5}{2(1-r)^4}-\frac{1}{6}(1-r)\theta'^2+\frac{1}{6}\theta\theta'^2$$
$$+\frac{1}{90}(1-r)^3\theta''^2-\frac{1}{45}(1-r)^3\theta'\theta'''-\frac{1}{6(1-r)}\theta^2\theta'^2$$
$$-\frac{1}{45}(1-r)^2\theta'^2\theta''+\frac{1}{90}(1-r)^2\theta\theta''^2-\frac{1}{45}(1-r)^2\theta\theta'\theta'''$$
$$-\frac{1}{945}(1-r)^5\theta'''^2+\frac{2}{945}(1-r)^5\theta''\theta^{(4)}$$
$$-\frac{2}{945}(1-r)^5\theta'\theta^{(5)}\Big]=O(\varepsilon^6). \tag{32}$$

To obtain the solitary wave solution, the velocity of the streams should be supercritical, which means the Froude number is greater than 1 in the nondimensional sense. The definition of Froude number is

$$\frac{U_i^2}{(1-\delta)\frac{(r-1)}{(r-1)+\delta}}=F_i^2,\quad i=1,2. \tag{33}$$

When $F_1=F_2=F$, we have

$$F^2(1-\delta)\frac{(r-1)}{(r-1)+\delta}+\frac{1}{2}+\delta F^2(1-\delta)\frac{(r-1)}{(r-1)+\delta}(r-1)$$
$$+\frac{1}{2}\delta(r-1)^2-\left(\frac{1}{2}F^2(1-\delta)\frac{(r-1)}{(r-1)+\delta}+1\right)(\theta+1)$$
$$+\frac{1}{2}(\theta+1)^2-F^2(1-\delta)\frac{(r-1)}{(r-1)+\delta}\Big[\frac{1}{2}-\frac{\theta}{2}+\frac{\theta^2}{2}-\frac{\theta^3}{2}$$
$$+\frac{\theta^4}{2}-\frac{\theta^5}{2}-\frac{1}{6}\theta'^2+\frac{1}{6}\theta\theta'^2+\frac{1}{90}\theta''^2-\frac{1}{45}\theta'\theta'''-\frac{1}{6}\theta^2\theta'^2$$
$$-\frac{1}{45}\theta'^2\theta''+\frac{1}{90}\theta\theta''^2-\frac{1}{45}\theta\theta'\theta'''-\frac{1}{945}\theta'''^2$$
$$+\frac{2}{945}\theta''\theta^{(4)}-\frac{2}{945}\theta'\theta^{(5)}\Big]-\frac{1}{2}\delta(\theta+1-r)^2$$
$$-\left(\frac{1}{2}\delta F^2(1-\delta)\frac{(r-1)}{(r-1)+\delta}+\delta g(1-r)\right)(r-(\theta+1))$$
$$+\delta F^2(1-\delta)\frac{(r-1)}{(r-1)+\delta}\Big[\frac{(1-r)}{2}-\frac{\theta}{2}+\frac{\theta^2}{2(1-r)}$$
$$-\frac{\theta^3}{2(1-r)^2}+\frac{\theta^4}{2(1-r)^3}-\frac{\theta^5}{2(1-r)^4}-\frac{1}{6}(1-r)\theta'^2$$
$$+\frac{1}{6}\theta\theta'^2+\frac{1}{90}(1-r)^3\theta''^2-\frac{1}{45}(1-r)^3\theta'\theta'''$$
$$-\frac{1}{6(1-r)}\theta^2\theta'^2-\frac{1}{45}(1-r)^2\theta'^2\theta''+\frac{1}{90}(1-r)^2\theta\theta''^2$$
$$-\frac{1}{45}(1-r)^2\theta\theta'\theta'''-\frac{1}{945}(1-r)^5\theta'''^2$$
$$+\frac{2}{945}(1-r)^5\theta''\theta^{(4)}-\frac{2}{945}(1-r)^5\theta'\theta^{(5)}\Big]=O(\varepsilon^6). \tag{34}$$

2.2. Perturbation solutions

We expand all the variables in terms of ε. And we stretch x coordinate in the same way as that by Fenton [9], which was originally introduced by Lighthill [27]. The perturbation schemes are outlined as follows

$$\theta(\alpha x)=\varepsilon\theta_1+\varepsilon^2\theta_2+\varepsilon^3\theta_3+O(\varepsilon^4), \tag{35}$$

$$F^2=1+\varepsilon F_{e1}+\varepsilon^2F_{e2}+\varepsilon^3F_{e3}+O(\varepsilon^4), \tag{36}$$

$$\alpha^2=\frac{((1-r)^2-\delta)}{(r-1)^2(1+(r-1)\delta)}(\varepsilon\alpha_1+\varepsilon^2\alpha_2+\varepsilon^3\alpha_3)+O(\varepsilon^4). \tag{37}$$

It should be noted that the subscripts in the perturbation expansions have nothing to do with the layers mentioned in last section. We substitute Eqs. (35)–(37) into Eq. (34) and rearrange all the terms in terms of the order of ε. We find that the terms containing ε^0, ε^1, ε^2 are eliminated. The coefficient of ε^3 is

$$\frac{(1-\delta)\big((1-r)^2-\delta\big)}{2(r-1)((r-1)+\delta)}$$
$$\times\left[\theta_1^3-\frac{(r-1)((r-1)+\delta)}{\big((1-r)^2-\delta\big)}F_{e1}\theta_1^2+\frac{1}{3}\alpha_1\theta_1'^2\right]. \tag{38}$$

The prime denotes the differentiation with respect to αx. To ensure the terms of $O(\varepsilon^3)$ vanish, we have the equation

$$\theta_1^3-\frac{(r-1)((r-1)+\delta)}{\big((1-r)^2-\delta\big)}F_{e1}\theta_1^2+\frac{1}{3}\alpha_1\theta_1'^2=0. \tag{39}$$

This is the familiar first-order KdV equation. We seek for the normal solitary solution, which is of smooth convex-shape without sharp corner. The maximum displacement is on the symmetry axis and the crest is rounded other than cusped. Using the conditions $\theta=\varepsilon$ and $\theta'=0$ at the crest, we can determine the Froude Number:

$$F_{e1}=\frac{((1-r)^2-\delta)}{(r-1)((r-1)+\delta)}. \tag{40}$$

The solution should also be uniformly valid, in which all the terms vanish as $|x|\to\infty$. This leads to the determination of α_1, *e.g.*,

$$\alpha_1=\frac{3}{4}. \tag{41}$$

Thus

$$\theta_1=\operatorname{sech}^2\sqrt{\frac{3}{4}\varepsilon\frac{\big((1-r)^2-\delta\big)}{(r-1)^2(1+\delta(r-1))}}(x-x_0), \tag{42}$$

where x_0 represents the position of the wave peak. In our coordinate system, it turns out to be $x_0=0$. In the following expressions, x_0 will be omitted.

The first-order solution above agrees with that given by Long [29], Benjamin [3] and Mirie and Su [31]. When $\rho_1 \simeq \rho_2$, it agrees with the results given by Keulegan [21] and Osborne and Burch [34]. If $\rho_2 = 0$, the solution becomes the surface solitary wave solution on one homogenous fluid. It agrees with the first-order solution given by Boussinesq [6], Korteweg and De Vries [23] and Fenton [9].

At the order of ε^4, it gives

$$\begin{aligned}
&\frac{(1-\delta)\big((1-r)^2-\delta\big)}{3(r-1)((r-1)+\delta)}\alpha_1\theta_1'\theta_2' \\
&+\left[\frac{3(1-\delta)\big((1-r)^2-\delta\big)}{2(r-1)((r-1)+\delta)}\theta_1^2-(1-\delta)F_{e1}\theta_1\right]\theta_2 \\
&+\frac{(1-\delta)\big((1-r)^2-\delta\big)}{6(r-1)((r-1)+\delta)}\alpha_2\theta_1'^2-\frac{1}{2}(1-\delta)F_{e2}\theta_1^2 \\
&+\frac{(1-\delta)\big((1-r)^2-\delta\big)}{6(r-1)((r-1)+\delta)}F_{e1}\alpha_1\theta_1'^2+\frac{1}{90}\alpha_1^2 \\
&\times\big(2\theta_1'\theta_1'''-\theta_1''^2\big)\frac{(1-\delta)\big((1-r)^2-\delta\big)^2\big(1-(1-r)^3\delta\big)}{(r-1)^3((r-1)+\delta)(1+(r-1)\delta)^2} \\
&+\frac{(1-\delta)((1-r)^3-\delta)}{2(r-1)^2((r-1)+\delta)}\theta_1^4+\frac{(1-\delta)\big((1-r)^2-\delta\big)}{2(r-1)((r-1)+\delta)}F_{e1}\theta_1^3 \\
&-\frac{(1-\delta)^2\big((1-r)^2-\delta\big)}{6(r-1)((r-1)+\delta)(1+(r-1)\delta)}\alpha_1\theta_1\theta_1'^2=0. \quad (43)
\end{aligned}$$

After we substitute the first-order solution into Eq. (43), it becomes an inhomogeneous ordinary differential equation with respect to θ_2. Again, we apply the restrictions at the crest, $\theta = \varepsilon$ and $\theta' = 0$. In other words, $\theta_1(0) = 1$, $\theta_1'(0) = 0$,$\theta_2(0) = 0$ and $\theta_2'(0) = 0$. Substituting them into Eq. (43), F_{e2} can be obtained as

$$\begin{aligned}
F_{e2} = &-(1-\delta)(20(r-1)((r-1)^2-\delta)^2 \\
&-20(r-1)((r-1)+\delta)((r-1)^3+\delta) \\
&-(((r-1)+\delta)((r-1)^2-\delta)^2(1+(r-1)^3\delta))/ \\
&(1+(r-1)\delta)^2)/(20(r-1)^3(-1+\delta)((r-1)+\delta)^2). \quad (44)
\end{aligned}$$

Together with the first-order component, the second-order solution agrees with the second-order internal solitary wave speed given by Long [29].

The abbreviation of Eq. (43) could be written as

$$\theta_2' + p(x)\theta_2 = q(x). \quad (45)$$

Here $p(x)$ and $q(x)$ are functions of x. The second-order component can be obtained by the standard procedure for the ordinary differential equation, which leads to

$$\theta_2 = \frac{\int e^{\int p(x')dx'}q(x)dx + C_0}{e^{\int p(x')dx'}}, \quad (46)$$

where C_0 is an arbitrary constant. When we substitute all the known variables including Eq. (44) for F_{e2} into Eq. (46), it yields

$$\begin{aligned}
\theta_2 = &C_0 \cdot \mathrm{sech}^2(\alpha x)\tanh(\alpha x) + C_1 \cdot \mathrm{sech}^2(\alpha x)\tanh^2(\alpha x) \\
&+C_2 \cdot x\mathrm{sech}^2(\alpha x)\tanh(\alpha x), \quad (47)
\end{aligned}$$

where

$$\begin{aligned}
C_1 = &-3(3(r-1)^4+(-9+33r-57r^2+81r^3-89r^4 \\
&+59r^5-21r^6+3r^7)\delta+(9-30r+48r^2-24r^3 \\
&-10r^4+14r^5-4r^6)\delta^2+3(r-1)^3\delta^3)/ \\
&\big(12(r-1)^2\big((r-1)^2-\delta\big)(1+(r-1)\delta)^2\big), \quad (48)
\end{aligned}$$

$$\begin{aligned}
C_2 = &((15+16\alpha_2)(r-1)^4+(r-1) \\
&\times(16\alpha_2(3-9r+12r^2-8r^3+2r^4) \\
&+3(15-40r+63r^2-52r^3+23r^4-6r^5+r^6))\delta \\
&+(16\alpha_2(r-1)^3\big(-3+3r-3r^2+r^3\big) \\
&+3(15-50r+88r^2-100r^3+70r^4-26r^5+4r^6))\delta^2 \\
&-(-15+16\alpha_2(r-1))\delta^3)/ \\
&\big(12(r-1)^2\big((r-1)^2-\delta\big)(1+(r-1)\delta)^2\big). \quad (49)
\end{aligned}$$

Since $\theta_2'(0) = 0$, Eq. (47) yields $C_0 = 0$.

The last term on the right hand side (RHS) of Eq. (47), which contains $x \cdot \mathrm{sech}^2(\alpha x)\tanh(\alpha x)$, attenuates much more slowly than the others without the multiplier x as $|x| \to \infty$. We have to manage to eliminate this term for the sake of uniform validity. By setting $C_2 = 0$, the unknown α_2 can be obtained explicitly as

$$\begin{aligned}
\alpha_2 = &-3(5(r-1)^4+(-15+55r-103r^2+115r^3-75r^4 \\
&+29r^5-7r^6+r^7)\delta+(15-50r+88r^2-100r^3 \\
&+70r^4-26r^5+4r^6)\delta^2+5(r-1)^3\delta^3)/ \\
&\big(16(r-1)^2\big((r-1)^2-\delta\big)(1+(r-1)\delta)^2\big). \quad (50)
\end{aligned}$$

The last unknown second-order component is then given by

$$\theta_2 = C_1 \cdot \mathrm{sech}^2(\alpha x)\tanh^2(\alpha x). \quad (51)$$

The second-order solution agrees with that given by Koop and Butler [22], Gear and Grimshaw [11] and Mirie and Su [31]. Again if $\rho_2 = 0$, the solution is reduced to the second-order solution for the surface solitary wave given by Laitone [26] and Fenton [9].

The same procedure can be used on the coefficients of ε^5. The ordinary differential equation for θ_3 is

$$\begin{aligned}
&C_3\alpha_1\theta_1'\theta_3'+C_4\theta_1^2\theta_3+C_5F_{e1}\theta_1\theta_3+C_6\alpha_1\theta_2'^2+C_7\alpha_2\theta_1'\theta_2' \\
&+C_8\alpha_3\theta_1'^2+C_9F_{e1}\alpha_1\theta_1'\theta_2'+C_{10}F_{e1}\alpha_2\theta_1'^2+C_{11}F_{e2}\alpha_1\theta_1'^2 \\
&+C_{12}\theta_1\theta_2^2+C_{13}F_{e1}\theta_2^2+C_{14}F_{e2}\theta_1\theta_2+C_{15}F_{e3}\theta_1^2+C_{16}\alpha_1^2\theta_1'\theta_2''' \\
&+C_{17}\alpha_1^2\theta_2'\theta_1'''+C_{18}\alpha_1^2\theta_1''\theta_2''+C_{19}\alpha_1^2\theta_1\theta_1'\theta_1'''+C_{20}\alpha_1^2\theta_1\theta_1''^2 \\
&+C_{21}\alpha_1^2\theta_1'^2\theta_1''+C_{22}F_{e1}\alpha_1^2\theta_1'\theta_1'''+C_{23}F_{e1}\alpha_1^2\theta_1''^2+C_{24}\alpha_1\alpha_2\theta_1'\theta_1''' \\
&+C_{25}\alpha_1\alpha_2\theta_1''^2+C_{26}\alpha_1^3\theta_1'\theta_1^{(5)}+C_{27}\alpha_1^3\theta_1''\theta_1^{(4)}+C_{28}\alpha_1^3\theta_1'''^2 \\
&+C_{29}\alpha_2\theta_1'^2\theta_1+C_{30}\alpha_1\theta_1'\theta_2''\theta_1+C_{31}\alpha_1\theta_1'^2\theta_1^2+C_{32}\theta_1^5 \\
&+C_{33}\alpha_1\theta_1'^2\theta_2+C_{34}\theta_1^3\theta_2+C_{35}\alpha_1\theta_1'^2\theta_1F_{e1}+C_{36}\theta_1^4F_{e1} \\
&+C_{37}\theta_1^2\theta_2F_{e1}+C_{38}\theta_1^3F_{e2}=0. \quad (52)
\end{aligned}$$

The constant coefficients $C_3 - C_{38}$ have been listed in Appendix C. In Eq. (52) θ_1, θ_2, F_{e1} and F_{e2} are known. In the same way used for the second-order components, we can obtain the rest third-order components for Froude number, α and wave profile, respectively, as follows

$$\begin{aligned}F_{e3} = {} & [-6(-1+r)^8 + (-1+r)^4(42 - 156r + 22r^2 + 68r^3 \\ & - 439r^4 + 680r^5 - 567r^6 + 274r^7 - 72r^8 + 8r^9)\delta \\ & + (-1+r)^3(126 - 558r + 8r^2 + 1500r^3 - 2667r^4 \\ & + 3257r^5 - 2709r^6 + 1371r^7 - 431r^8 + 85r^9 - 11r^{10} \\ & + r^{11})\delta^2 + (-1+r)^2(210 - 1080r + 340r^2 + 4864r^3 \\ & - 10590r^4 + 11180r^5 - 8211r^6 + 4964r^7 - 2342r^8 \\ & + 764r^9 - 158r^{10} + 16r^{11})\delta^3 + (-210 + 1440r \\ & - 2320r^2 - 4936r^3 + 25764r^4 - 47716r^5 + 51415r^6 \\ & - 36658r^7 + 18873r^8 - 7548r^9 + 2319r^{10} - 466r^{11} \\ & + 43r^{12})\delta^4 + (126 - 828r + 1358r^2 + 2748r^3 \\ & - 15759r^4 + 31708r^5 - 36570r^6 + 26256r^7 - 11740r^8 \\ & + 3116r^9 - 444r^{10} + 28r^{11})\delta^5 + (-42 + 264r - 508r^2 \\ & - 332r^3 + 3631r^4 - 8366r^5 + 10668r^6 - 8426r^7 \\ & + 4119r^8 - 1148r^9 + 140r^{10})\delta^6 + 6(-1+r)^6\delta^7]/ \\ & (140(-1+r)^5((-1+r)+\delta)^3(1+(-1+r)\delta)^4),\end{aligned} \tag{53}$$

$$\begin{aligned}\alpha_3 = {} & (3(30(-1+r)^6 + (-1+r)^2(-150 + 600r - 1234r^2 \\ & + 1392r^3 - 903r^4 + 346r^5 - 83r^6 + 12r^7)\delta + (300 \\ & - 1800r + 5502r^2 - 10800r^3 + 14451r^4 - 13496r^5 \\ & + 8970r^6 - 4348r^7 + 1580r^8 - 436r^9 + 88r^{10} \\ & - 12r^{11} + r^{12})\delta^2 + (-300 + 1800r - 5502r^2 + 11220r^3 \\ & - 16341r^4 + 17152r^5 - 12946r^6 + 7016r^7 - 2720r^8 \\ & + 740r^9 - 132r^{10} + 12r^{11})\delta^3 + (-1+r)^3(-150 \\ & + 450r - 784r^2 + 1028r^3 - 925r^4 + 501r^5 - 152r^6 \\ & + 20r^7)\delta^4 - 30(-1+r)^6\delta^5))/(80(-1+r)^4 \\ & \times((-1+r)^2 - \delta)(1+(-1+r)\delta)^4),\end{aligned} \tag{54}$$

$$\begin{aligned}\theta_3 = {} & (\operatorname{sech}^4(\alpha x)\cdot\tanh^2(\alpha x)(5\cosh(2\alpha x)(15(-1+r)^8 \\ & + 2(-1+r)^4(-45 + 165r - 297r^2 + 465r^3 - 478r^4 \\ & + 297r^5 - 102r^6 + 15r^7) + (-1+r)^2(225 - 1200r \\ & + 3216r^2 - 6108r^3 + 9329r^4 - 11540r^5 + 11322r^6 \\ & - 8640r^7 + 4997r^8 - 2100r^9 + 606r^{10} - 108r^{11} \\ & + 9r^{12})\delta^2 - 2(-1+r)^2(150 - 750r + 1962r^2 \\ & - 3348r^3 + 4632r^4 - 5328r^5 + 4569r^6 \\ & - 2664r^7 + 995r^8 - 218r^9 + 21r^{10})\delta^3 + (225 - 1500r \\ & + 4866r^2 - 9552r^3 + 12452r^4 - 11324r^5 + 7542r^6 \\ & - 4000r^7 + 1884r^8 - 800r^9 + 272r^{10} - 64r^{11} + 8r^{12})\delta^4 \\ & + 2(-1+r)^3(45 - 150r + 252r^2 - 120r^3 - 137r^4 \\ & + 213r^5 - 108r^6 + 20r^7)\delta^5 + 15(-1+r)^6\delta^6) \\ & - 2(114(-1+r)^8 - (-1+r)^4(684 - 2508r + 3876r^2 \\ & - 2766r^3 - 541r^4 + 3954r^5 - 4341r^6 + 2358r^7 - 648r^8 \\ & + 72r^9)\delta + (-1+r)^2(1710 - 9120r + 21888r^2 \\ & - 30156r^3 + 23132r^4 - 7496r^5 + 2295r^6 - 7968r^7 \\ & + 10922r^8 - 7266r^9 + 2694r^{10} - 540r^{11} + 45r^{12})\delta^2 \\ & - (2280 - 15960r + 51072r^2 - 98952r^3 + 127272r^4 \\ & - 109680r^5 + 48867r^6 + 26220r^7 - 73580r^8 + 72102r^9 \\ & - 41802r^{10} + 14948r^{11} - 3063r^{12} + 276r^{13})\delta^3 + (1710 \\ & - 11400r + 34428r^2 - 63324r^3 + 78338r^4 - 63224r^5 \\ & + 27495r^6 - 778r^7 - 3939r^8 - 530r^9 + 2057r^{10} \\ & - 928r^{11} + 140r^{12})\delta^4 + (-684 + 4332r - 12084r^2 \\ & + 20034r^3 - 21593r^4 + 16038r^5 - 9456r^6 + 5368r^7 \\ & - 2739r^8 + 924r^9 - 140r^{10})\delta^5 + 114(-1+r)^6\delta^6))) / \\ & (240(-1+r)^4(-(-1+r)^2\rho_1 + \rho_2)^2 \\ & \times(\rho_1 + (-1+r)\rho_2)^4).\end{aligned} \tag{55}$$

The horizontal velocities on the bottom and the top can be calculated by Eqs. (27) and (28) after substituting the wave profile.

2.3. Verification

Mirie and Su [31] presented the expressions of the third-order solution of an internal solitary wave in a rigid-lid two-layer model. The expressions include the wave speed, interface displacement and horizontal bottom and ceiling velocities. Mirie and Pennell [30] studied further the properties of internal solitary waves based on the ninth-order perturbation solution. However, in the paper by Mirie and Pennell [30], they did not give out the explicit expressions. Therefore, the solution given by Mirie and Su [31] is chosen for comparison with the third-order solution in the present paper.

As mentioned before, if the density of the upper layer is set to be zero, the solution of a surface solitary wave on a homogenous fluid emerges from the internal solitary wave solution. The surface solitary wave solution yielded from the third-order internal solitary wave solution both in the present paper and that of Mirie and Su [31] have been compared with those given by other authors. It is found that both of the solutions are identical with that of Grimshaw [12] and Fenton [9]. However, if the density in the upper layer is not zero, θ, F and α obtained in this paper are different from those given by Mirie and Su [31].

There is a specific example in the paper by Mirie and Pennell [30], which gave F^2 for $r = 1.5$ and $\delta = 0.05$ up to the ninth order. The third-order solution taken from Eq. (29) in their paper is

$$F^2 = 1 + (8/11)\varepsilon - (784786/1017005)\varepsilon^2 - 1.206\varepsilon^3. \tag{56}$$

With the same parameters, the solution given by the present paper yields

$$F^2 = 1 + \frac{8}{11}\varepsilon - \frac{784786}{1017005}\varepsilon^2 - \frac{157802664378}{131638076185}\varepsilon^3. \tag{57}$$

$157802664378/131638076185 \approx 1.20584,$

which is virtually the same as 1.206.

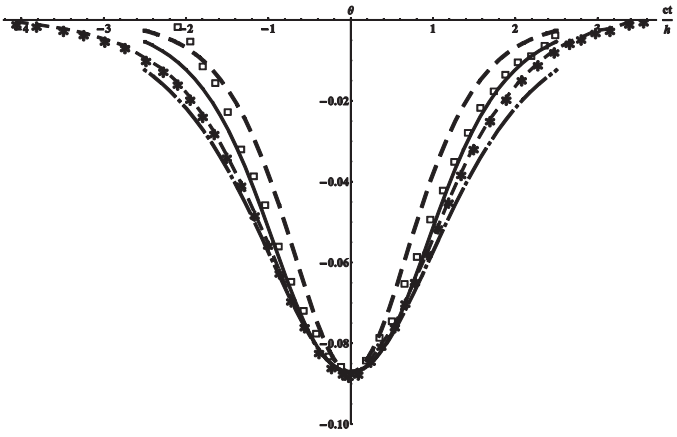

Fig. 2. Internal solitary wave profiles for $r = 5.13/4.13$, $\delta = 999/1022$ and $\varepsilon = -0.087$. The dashed line (- - -) is the first-order solution; the dot dashed (- · -) line is the second-order solution; the solid line (—) is the third-order solution in the present paper. The □ is experimental measurement given by Grue et al. [13]. The asterisk dashed line (-∗-) is the numerical solution given by Grue et al. [13]. (Data have been extracted from Fig. 7(b) in their paper and converted to the same units used in the present paper.)

The expression in the paper by Mirie and Su [31] gives

$$F^2 = 1 + \frac{8}{11}\varepsilon - \frac{784786}{1017005}\varepsilon^2 - \frac{158734610778}{131638076185}\varepsilon^3. \tag{58}$$

$158734610778/131638076185 \approx 1.19876$,

which does not agree with the corresponding coefficient in Eq. (56).

Furthermore, the solution in the present work and that of Mirie and Su [31] have been substituted back to the continuity equations and Bernoulli equations, which were Eqs. (1)–(3) in the paper by Mirie and Su [31]. It was found that, with the solution in the present paper, the residual of continuity and Bernoulli equations is of the order $O(\varepsilon^{7/2})$. Whereas residual of the order $O(\varepsilon^3)$ remains when the solution given by Mirie and Su [31] is used. Therefore, it can be concluded that the expressions given by Mirie and Su [31] do not satisfy the governing equations up to the third order but the solution in the present paper satisfies the same governing equations up to the third order.

2.4. Validation

The first- to third-order solutions have also been compared with the numerical solution of the fully nonlinear model and the experimental measurement given by Grue et al. [13] (Fig. 2). The third-order solution agrees with the experiment better than the first- and second-order solutions.

3. Numerical simulations based on the Euler equations

3.1. Mathematical model

Fluids are assumed to be incompressible and inviscid in the CFD simulations of internal solitary waves. The N–S equations can be then reduced to the Euler equations. In this paper, no surface tension is taken into account based on the assumption that the curvature of the wave profile is small. The continuity and momentum equations are

$$\nabla \cdot \mathbf{u} = 0, \tag{59}$$

$$\frac{\partial}{\partial t}(\rho \mathbf{u}) + \nabla \cdot (\rho \mathbf{u}\mathbf{u}) = -\nabla p - \rho \mathbf{g}. \tag{60}$$

where $\mathbf{u}$ is the vector-valued fluid velocity, $\mathbf{g}$ is a vector for the gravitational acceleration, ρ is the density and p is pressure.

In order to implement the VOF method for capturing the free interface, an indicator scalar field is introduced. α_1 is designated as the volume fraction in an infinitesimal element of the dense phase, referring to dense water in a two-layer system. $\alpha_1 = 1$ indicates the dense fluid and $\alpha_1 = 0$ indicates the other. The transition from 0 to 1 implies the interface. α_1 is driven by the flow. It results in the advection equation [40]:

$$\frac{\partial \alpha_1}{\partial t} + \nabla \cdot \mathbf{u}\alpha_1 = 0. \tag{61}$$

The density field is determined by the weighted average of all the phases, that is,

$$\rho = \alpha_1 \rho_1 + (1 - \alpha_1)\rho_2, \tag{62}$$

where ρ_1 and ρ_2 are the densities of the dense and light phases, respectively.

Special attention should be paid to the smeared interface due to the numerical diffusion. The method used in OpenFOAM is different from the geometrical methods, such as Simple Line Interface Calculation (SLIC) method [32] and Piecewise-Linear Interface Calculation (PLIC) method [24], or the higher order differencing schemes, such as Compressive Interface Capturing Scheme for Arbitrary Meshes (CICSAM) [40]. Inspired by the two-fluid Eulerian model, Eq. (61) is replaced by [38]

$$\frac{\partial \alpha_1}{\partial t} + \nabla \cdot \mathbf{u}\alpha_1 + \nabla \cdot [\mathbf{u}_r \alpha_1 (1 - \alpha_1)] = 0, \tag{63}$$

in which $\mathbf{u}_r$ is designated as the "compression velocity" [5]. The "compression term", the third term on the left hand side (LHS) of Eq. (63), is zero when $\alpha_1 = 0$ **or** 1. Thus, if the interface is theoretically a step-profile, Eq. (63) degenerates to Eq. (61). The functionality of the "compression term" is to compress the transitional layer where $0 < \alpha_1 < 1$. The "compression strength" can be adjusted by the constant C_α, which appears in the definition of the magnitude of $\mathbf{u}_r$, $|\mathbf{u}_r| = \min[C_\alpha |\mathbf{u}|, \max(|\mathbf{u}|)]$. The direction of $\mathbf{u}_r$ is perpendicular to the interface. $C_\alpha = 0$ yields no compression; $C_\alpha = 1$ yields a conservative compression; $C_\alpha > 1$ yields enhanced compression. In this study, it is set to be 1 as default [15].

In OpenFOAM, a pseudo-dynamic pressure is defined by

$$p_{rgh} = p - \rho \mathbf{g} \cdot \mathbf{x}, \tag{64}$$

where $\mathbf{x}$ is the position vector. Eq. (60) can be written as

$$\frac{\partial}{\partial t}(\rho \mathbf{u}) + \nabla \cdot (\rho \mathbf{u}\mathbf{u}) = -\nabla p_{rgh} - \mathbf{g} \cdot \mathbf{x} \nabla \rho. \tag{65}$$

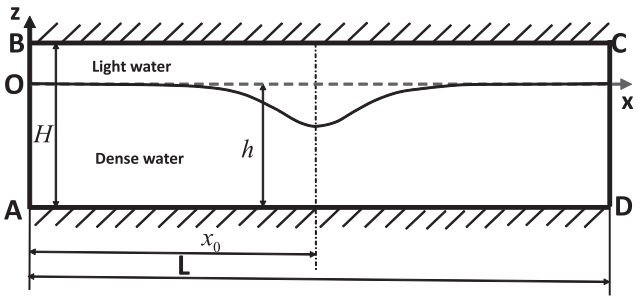

Fig. 3. Computational domain in the 2D simulations for internal solitary waves.

Eqs. (59), (63) and (65) form a closed set of governing equations [38].

3.2. Numerical procedure

The time marching is achieved by implicit Euler scheme. The spatial terms are discretised by the Finite Volume Method (FVM) on a structured mesh. Utilising Gauss' theorem, the integrals of a volume can be transferred to integrals over the faces of a cell. The velocity gradient on the LHS of Eq. (59) is evaluated by the linear face interpolation [19]. The convection term in Eq. (65) is discretised by the second-order Total Variation Diminishing (TVD) limited linear scheme [14]. The Modified Upwind Scheme for Conservation Laws (MUSCL) scheme is applied to discretise second term on the LHS of Eq. (63) [41]. The discretisation scheme for the "compression term" in Eq. (63) is called "interfaceComprssion" in OpenFOAM, which has been introduced in detail by Berberović et al. [5]. The source terms on the RHS of Eq. (65) are linearised and then integrated over a control volume. The boundedness of α_1 is achieved by the Multidimensional Universal Limiter for Explicit Solution (MULES) algorithm [38]. The coupled pressure–velocity field depicted by Eqs. (59) and (65) is solved by the PISO-SIMPLE (PIMPLE) algorithm [33], which is a combination of Semi-Implicit Method for Pressure-Linked Equations (SIMPLE) algorithm [37] and Pressure Implicit with Splitting of Operator (PISO) algorithm [17]. One can refer to the paper by Higuera et al. [15] for the flow chart of the PIMPLE algorithm. The assembled linear system of equations in terms of p_{rgh} is solved by the Geometric-Algebraic Multi-Grid (GAMG) with Gauss–Siedel smoother solver [2]. The linear system of equations in terms of $\mathbf{u}$ is solved by the Preconditioned Bi-Conjugate Gradient (PBiCG) solver with Diagonal based Incomplete LU (DILU) preconditioner [43].

3.3. Computational domains and configurations

The 2D computational domain for internal solitary waves (Fig. 3) resembles a rectangular wave tank. The Cartesian coordinate system O-xz is defined in the domain. The z-axis points to the vertically upward orientation. The wave travels along the x-axis horizontally. And the x-axis is located on the undisturbed interface. The gravitational acceleration throughout the paper is 9.81 m/s^2 in the $-z$ direction. The density of the light wave phase is 1000 kg/m^3 and the density of the dense water phase is 1025 kg/m^3. The initial location of the wave is x_0. The length of the wave tank is L and the total height is H. h is the depth of the undisturbed lower layer in the simulations of internal waves.

3.4. Wave generation by assigning initial conditions

Prior to the calculation, the velocity, pressure, phase fraction at any point should be initialised. Analytical solutions of the solitary waves are used to define the interface location of the two phases. The velocity field has to be assigned by the analytical solutions too. Since it is assumed to be incompressible flow, the pressure can be determined by the velocity. The initial pressure field only affects the convergence speed within the first time step. Therefore, the pressure is assigned to be zero for convenience.

It is remarked that the analytical solutions are based on the potential theory. Nevertheless, the Euler equations can solve rotational flow. According to Stokes' theorem and Kelvin's circulation theorem, if the initial condition of in an inviscid fluid is irrotational flow, the flow field remains irrotational afterwards. In other words, the solution of Euler equations is potential flow when the initial condition is potential flow. The truncated perturbation solution of a solitary wave satisfies the Laplace equation exactly. However, it does not satisfy the irrotational flow criterion by leaving a higher-order residual. That fact does not violate the potential theory asymptotically. If the truncated solution is used as the initial condition for the calculation governed by the Euler equations, it results in a rotational flow. The simulation result has to be examined carefully. The physical definition, namely, permanent form and constant wave speed, can be used for the verification.

Special attention should be paid when implementing the solution of the MCC model. The MCC model only gives the implicit expressions of the wave profile and particle velocity with respect to the horizontal coordinate. In order to implement it in the code, interpolation has to be used. Taking into account the velocity, the value of the interpolation function and its first derivative should be continuous. Therefore, the piecewise cubic Hermite interpolation is adopted [25].

Suppose that there is a set of sequential data points (x_k, z_k), where $k = 1, \ldots, n$, and $x_k < x_{k+1}$. Let us consider the interpolation function $P(x)$ on the kth interval, in which $x_k < x < x_{k+1}$. Both the value and the first derivative of the function are required to coincide with the data, that is,

$$P(x_k) = z_k, \quad P(x_{k+1}) = z_{k+1}, \quad P'(x_k) = z'_k, \quad P'(x_{k+1}) = z'_{k+1}. \tag{66}$$

The length of the interval is donated as l_k, which is given by

$$l_k = x_{k+1} - x_k. \tag{67}$$

The first divided difference, δf_k, is defined as

$$\delta f_k = \frac{z_{k+1} - z_k}{l_k}. \tag{68}$$

The starting tangent and ending tangent are

$$d_k = P'(x_k),\ d_{k+1} = P'(x_{k+1}), \tag{69}$$

respectively. With the local distance, $s = x - x_k$, $P(x)$ can be written as

$$P(x) = \frac{3l_k s^2 - 2s^3}{l_k^3} z_{k+1} + \frac{l_k^3 - 3l_k s^2 + 2s^3}{l_k^3} z_k + \frac{s^2(s - l_k)}{l_k^2} d_{k+1} + \frac{s(s - l_k)^2}{l_k^2} d_k. \tag{70}$$

If we do not have the first derivative at each point, we need a method to determine the derivative. A "Shape-Preserving Piecewise Cubic" method proposed by Fritsch and Carlson [10] has been chosen, for it has been successfully implemented in MATLAB called "Piecewise Cubic Hermite Interpolating Polynomial" (PCHIP). There are several circumstances in order to decide the value of d_k:

(i) If $\delta f_{k-1} \cdot \delta f_k < 0$, or $\delta f_{k-1} \cdot \delta f_k = 0$, then $d_k = 0$.

(ii) If $\delta f_{k-1} \cdot \delta f_k > 0$, then d_k is given by the "weighted harmonic mean" of the neighbour slopes:

$$\frac{wh_1 + wh_1}{d_k} = \frac{wh_1}{\delta f_{k-1}} + \frac{wh_2}{\delta f_k}, \tag{71}$$

where

$$wh_1 = 2l_k + l_{k-1}, \quad wh_2 = l_k + 2l_{k-1}. \tag{72}$$

(iii) The derivatives at the endpoints (x_1, z_1) and (x_n, z_n) can be obtained by three-point extrapolation. But for this specific application for solitary waves, the derivatives at the endpoints can be simply assigned by 0 provided the displacement of interface is sufficiently small.

3.5. Boundary conditions

There are only two boundary conditions:

(i) "Slip-wall" boundary condition. It is used to model the rigid walls in the NWT. The mathematical expressions are

$$\mathbf{u} \cdot \mathbf{n} = 0, \quad \alpha_{1n} = 0, \quad p_n = 0, \tag{73}$$

where $\mathbf{n}$ is the normal vector of the wall and the subscript n means the normal derivative to the boundary.

(iii) "Cyclic" boundary condition. It consists of a pair of boundaries, for example, AB and CD shown in Fig. 3. The variables on the two boundaries stay the same to simulate a circulating water flume.

3.6. Time control

The time step in OpenFOAM can be adjusted adaptively. First the local Courant number is defined as

$$Co = \frac{|\mathbf{u}_f \cdot \mathbf{S}_f|}{\mathbf{d} \cdot \mathbf{S}_f} \Delta t, \tag{74}$$

where f implies the value of the variable in the middle of the face, $\mathbf{S}$ is the outward-pointing face area vector, Δt is time step and $\mathbf{d}$ is a vector between two centroids of the cells sharing the calculated surface. The maximum Courant number should not exceed the user defined value. For more subtle adjustment algorithm, one can refer to the introduction by Berberović et al. [5]. The courant number used in the simulation is set to be smaller than 0.2 anywhere.

Table 1
The parameters of the internal solitary wave cases (part 1).

Case	L	H	Grid quantity ($x \times z$)	Boundary condition of AB and CD
1	40	4/3	1000×120	Periodic
2	40	4/3	1000×120	Periodic
3	40	4/3	1000×120	Periodic
4	40	4/3	1000×120	Periodic
5	40	4/3	1000×120	Periodic
6	40	4/3	2000×240	Periodic
7	40	4/3	2000×240	Periodic
8	40	4/3	2000×240	Periodic
9	40	4/3	2000×240	Periodic
10	40	4/3	2000×240	Periodic
11	213.333	4/3	8192×384	Slip wall

4. Result analysis

4.1. Case study set-ups

11 numerical cases will be used to investigate simulations of a single internal solitary wave with various initial conditions. In this section, all the length variables or parameters are scaled by the depth of the undisturbed lower layer h, time is scaled by h/c_0 where c_0 is given by Eq. (21) and the densities are scaled by the density of the lower layer ρ_1. The common configurations are firstly introduced. The depth of the undisturbed upper layer is 1/3. The density of the upper layer is 1.025. The boundary conditions on the bottom (DA in Fig. 3) and on the top (BC in Fig. 3) are "slip walls". There are no relaxation zones. The horizontal cell sizes in the x direction are uniform. The grading ratio Rw is defined as the ratio between the size of the last cell and that of the first cell in a block. The grading ratios in the z direction are 0.2 and 5 in two blocks, which are below and above the undisturbed interface, respectively. Within the block, the cell sizes in the z direction are aligned with a geometric progression. The other parameters are listed in Tables 1 and 2.

4.2. Convergence study

The objective of this study is to investigate the influence of the initial condition on the propagation of the internal solitary wave in the CFD simulation. Therefore, the effect due to discretization and numerical diffusion should not be predominant in this study.

Case 6 has been chosen for the convergence study. The contour line where $\alpha_1 = 0.5$ is used to locate the interface in this section and hereinafter. The displacement of the trough

Table 2
The parameters of the internal solitary wave cases (part 2).

Case	Initial condition	Initial wave amplitude	Initial position of the trough	End time	Final position of the trough
1	1st-order KdV solution	−0.0667	13.333	11.402	25.080
2	2nd-order KdV solution	−0.0667	13.333	11.402	25.320
3	3rd-order KdV solution	−0.0667	13.333	11.402	25.320
4	eKdV solution	−0.0667	13.333	11.402	25.280
5	MCC solution	−0.0667	13.333	11.402	25.357
6	1st-order KdV solution	−0.1333	13.333	11.402	25.340
7	2nd-order KdV solution	−0.1333	13.333	11.402	26.039
8	3rd-order KdV solution	−0.1333	13.333	11.402	25.728
9	eKdV solution	−0.1333	13.333	11.402	25.740
10	MCC solution	−0.1333	13.333	11.402	25.960
11	3rd-order KdV solution	−0.1333	13.333	114.02	137.5

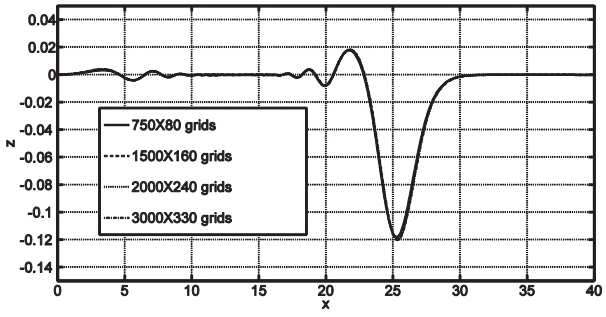

Fig. 4. The wave profiles of different runs in the spatial convergence study of Case 6 for the internal solitary wave at $t = 11.402$.

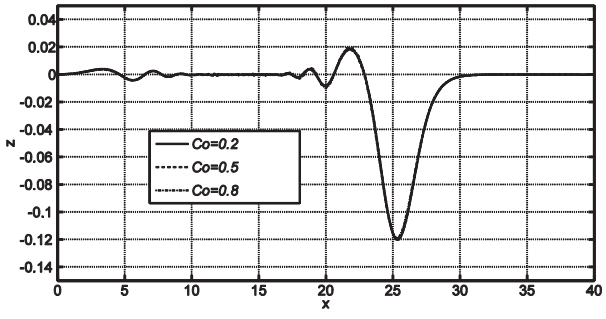

Fig. 5. The wave profiles of different runs in the temporal convergence study of Case 6 for the internal solitary wave at $t = 11.402$.

with respect to the still interface level a is used as a reference parameter. The wave profiles of different runs after they have propagated for $t = 11.402$ are shown in Figs. 4 and 5. $a = -0.1180$ in the run with 750×80 grids; $a = -0.1195$ in the run with 1500×80 grids; $a = -0.1202$ in the run with 2000×240 grids; $a = -0.1202$ in the run with 3000×330 grids. The wave profiles converge. And the difference between the wave amplitude in the run with the densest mesh and that of the sparsest mesh is 1.83%. The Courant number chosen in the study is also appropriate as shown in Fig. 5.

4.3. Case studies

Generally there are two obstacles preventing us from obtaining a genuine or ideal internal solitary wave in an inviscid numerical wave tank. One comes from the discretisation and numerical diffusion in order to circumvent the nonlinearity of the governing equations as well as the free interface boundary conditions. The other is due to the mismatching between the initial condition and the fully nonlinear solution. The objective of this study is to investigate the latter problem, that is, the influence of the initial condition on the propagation of the internal solitary wave in the CFD simulation.

Cases 1–10 are divided into two groups shown in Fig. 6 (Group 1) and Fig. 7 (Group 2), respectively, according to their initial wave amplitudes. It is remarked the depth of the upper layer is approximate 0.3333. The initial amplitude of Group 1 can be classified as small. The initial amplitude of Group 2 is much larger than that of Group 1. Nevertheless, it is still much smaller than the greatest amplitude. The current discussion is confined within the weakly nonlinear regime.

Within each group, the initial conditions are different. When the initial amplitude is small, the simulated wave profiles at different moments of all cases are closely similar to the initial profiles. They match the physical depicts of the solitary wave, that is, the permanent form and constant wave speed. However, when the initial amplitude is large as in Group 2, the wave profiles deviate from the initial forms. It can be clearly seen from the trajectory of the trough. In order to give a quantitative comparison, the wave amplitudes at the final time step of the cases have been extracted. The relative errors with respect to their initial amplitudes have been shown in Fig. 8, where cases have been labelled by their initial conditions. Among all the initial conditions, the third-order KdV solution performs the best to keep the wave form stable. It is easy to speculate that the lower-order KdV solutions result in bigger errors as the initial amplitude becomes larger. However, it was not expected that simulations initialised by the eKdV and MCC solutions produce larger errors as the initial amplitude becomes larger. It is probably owing to the incompatibility between the lower-order approximation of the velocity field and the fully nonlinear governing equations. Camassa et al. [7] have amended the local velocities. That is promising to improve the accuracy of the MCC model.

Case 11 simulated the wave propagating over a longer distance initialised by the third-order KdV solution. As shown in Fig. 9, the wave stays stable throughout. However, subtle difference can be distinguished according to the trajectory of the trough. The propagation can be roughly divided into two segments by the $t = 11.402$. Before that time, the variation of the amplitude is more violent. It manifests the mismatching between the initial condition and the fully nonlinear solution. After $t = 11.402$, the amplitude decays exponentially. It is due to the discretisation errors and numerical diffusion.

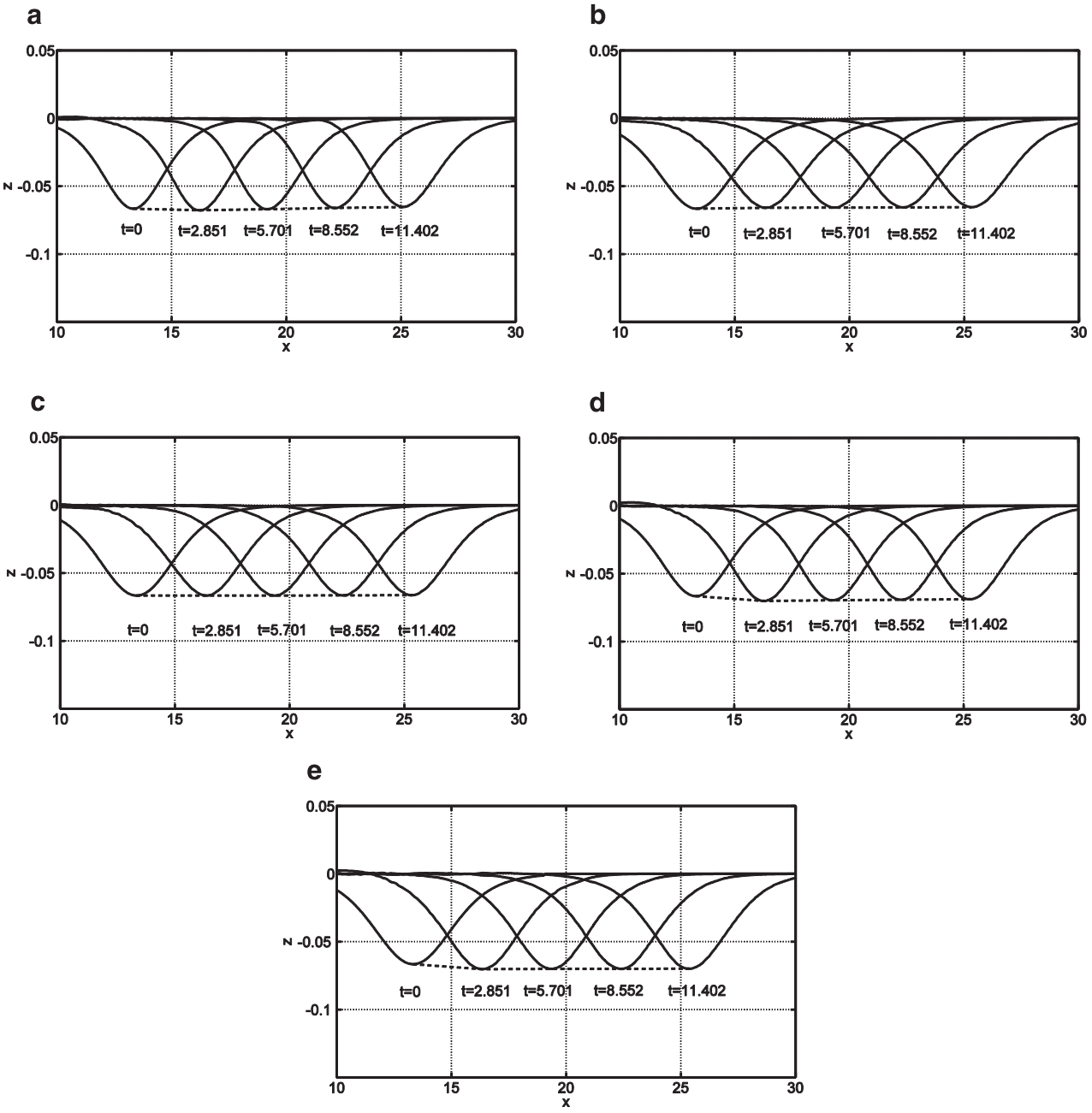

Fig. 6. The wave profiles at different moments given by Case 1 (a), Case 2 (b), Case 3 (c), Case 4 (d) and Case 5 (e). The dashed line connects the troughs in each plot.

Overall, the simulation initialised by the third-order KdV solution gives a satisfactory result.

5. Conclusions

This paper presented a novel derivation of the higher-order weakly nonlinear solutions for a single internal solitary wave. The conserved quantities reveal the mass conservations within each layer and the momentum transfer between two layers. The momentum transfer via the interface fundamentally differs from the mechanisms of surface waves. The successive approximation method has been used to derive equations to any accuracy. The partial differential equation in terms of the interface displacement has been converted to ordinary differential equations at each order via the perturbation method. The ordinary differential equations can be successively solved with additional restrictions. This method can be applied to seek for the KdV-type soliton solution up to any order. The third-order solution given by the present paper corrects an error by Mirie and Su [31]. It agrees better with the experiment than the lower-order solutions.

Various analytical solutions have been used to initialise the flow field in the CFD simulations of internal solitary waves.

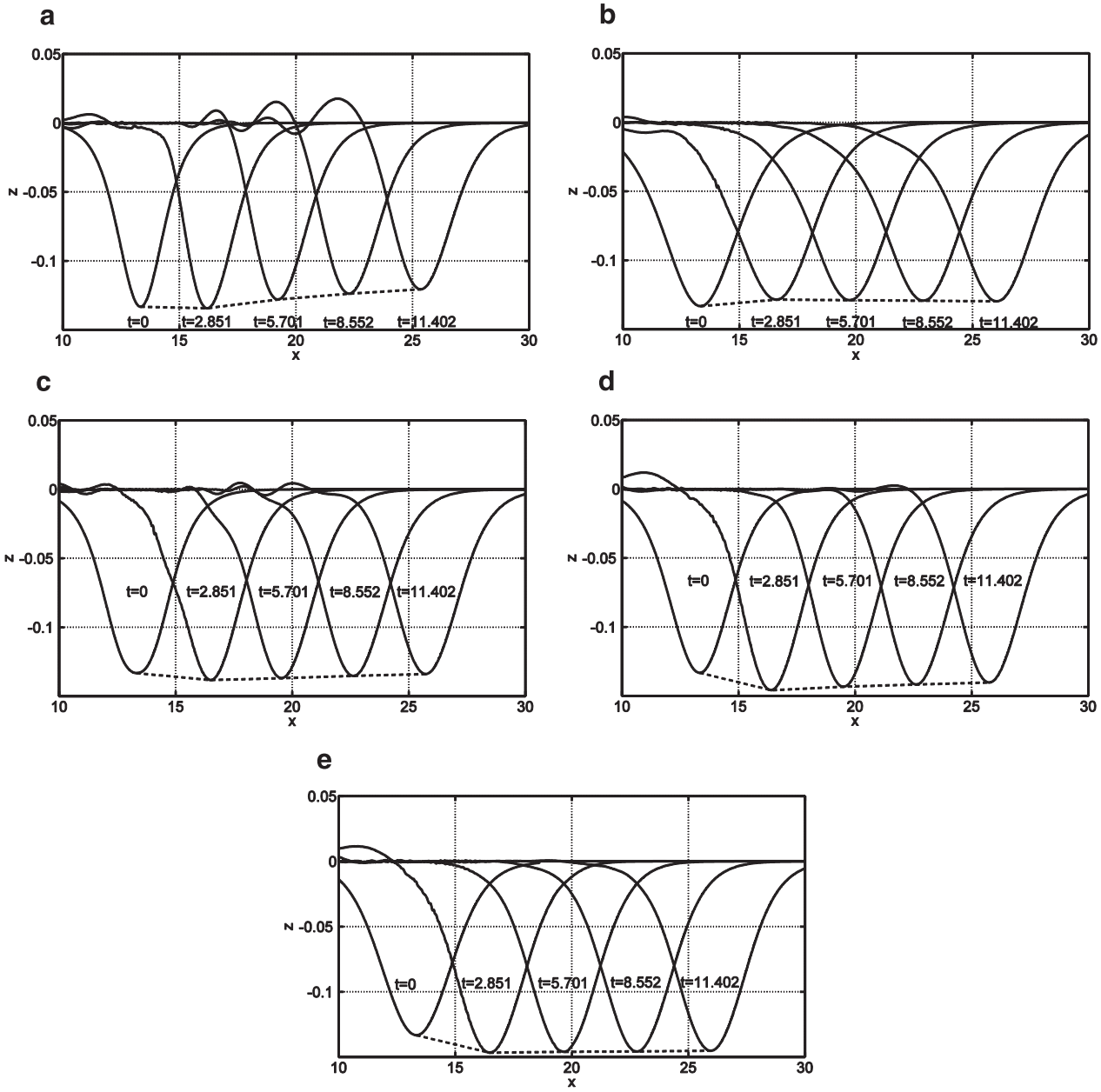

Fig. 7. The wave profiles at different moments given by Case 6 (a), Case 7 (b), Case 8 (c), Case 9 (d) and Case 10 (e). The dashed line connects the troughs in each plot.

Two main factors affect the accuracy with respect to a genuine solitary wave. The mismatch between the analytical solution and the fully nonlinear governing equations predominates in the incipient period and results in relatively severe wave profile variation. Numerical dissipation leads to mild attenuation. It has been observed that the third-order KdV solution results in the most stable internal solitary wave in the numerical wave tank both with small amplitude and finite amplitude. It proves reversely that the third-order KdV solution is the most precise soliton solution in that range. The conclusion will benefit more complicated simulations on internal solitary waves subsequently.

Acknowledgements

The authors would like to gratefully acknowledge G.X. Wu, Y. Semenov, Y. Chen, A. K. Liu, and R. Grimshaw for their genuine help. The authors acknowledge the use of the UCL Legion High Performance Computing Facility (Legion@UCL), and associated support services, in the completion of this work.

This work is supported by Lloyd's Register Foundation (LRF) through the joint centre involving University College London, Shanghai Jiaotong University and Harbin Engineering University, to which the authors are most grateful. Lloyd's

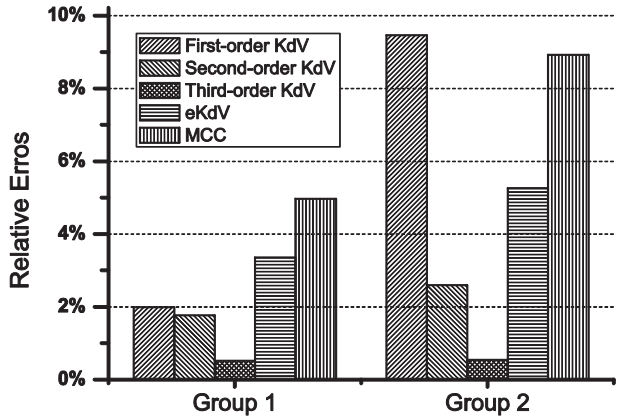

Fig. 8. The relative errors of the wave amplitudes at $t = 11.402$ with respect to their initial amplitude.

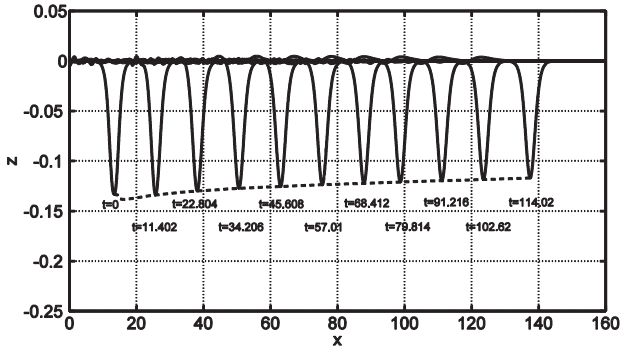

Fig. 9. The wave profiles in Case 11 at different moments. The dashed line shows the trajectory of the trough.

Register Foundation helps to protect life and property by supporting engineering-related education, public engagement and the application of research.

The first author acknowledges the scholarship sponsored by the Erasmus Mundus Europe Asia (EMEA) scholarship programme, Faculty of Engineering of University College London and the Henry Lester Trust Ltd. The second author acknowledges the financial support by the China Scholarship Council (CSC) (no. 201206680001).

Appendix A. Proving S to be constant

Substituting Eqs. (10) and (11) to Eq. (12), we have

$$S = \int_0^{\eta} \left(p_1 + \rho_1 u_1^2\right) dz + \int_{\eta}^{H} \left(p_2 + \rho_2 u_2^2\right) dz, \tag{A.1}$$

which is a function of a single independent variable x. It is noted that the upper limit of the integral in the first term, η, which is also the lower limit of the integral in the second term, is a function of a single independent variable x too. We assume both S and η are continuous and derivable everywhere while $x \in (-\infty, \infty)$. We take the derivative of S with respect to x, *viz.*,

$$\begin{aligned}\frac{dS}{dx} &= \int_0^{\eta} (p_{1x} + 2\rho_1 u_1 u_{1x}) dz \\ &\quad + \eta_x \left[p_1(x, \eta(x)) + \rho_1 u_1^2(x, \eta)\right] \\ &\quad + \int_{\eta}^{H} (p_{2x} + 2\rho_2 u_2 u_{2x}) dz \\ &\quad - \eta_x \left[p_2(x, \eta(x)) + \rho_2 u_2^2(x, \eta)\right],\end{aligned} \tag{A.2}$$

where the subscript x donates differentiation with respect to x. At the interface of two fluids, the pressure is continuous. Thus we have

$$p_1(x, \eta(x)) = p_2(x, \eta(x)). \tag{A.3}$$

The corresponding terms in Eq. (A.2) are cancelled out, *viz.*,

$$\eta_x p_1(x, \eta(x)) - \eta_x p_2(x, \eta(x)) = 0. \tag{A.4}$$

The momentum conservation equations in the two layers are

$$\begin{cases} -u_1 u_{1x} - w_1 u_{1y} = \dfrac{p_{1x}}{\rho_1}, \\ -u_2 u_{2x} - w_2 u_{2y} = \dfrac{p_{2x}}{\rho_2}. \end{cases} \tag{A.5}$$

Hence the pressure gradient can be expressed as

$$\begin{cases} p_{1x} = -\rho_1 u_1 u_{1x} - \rho_1 w_1 u_{1z}, \\ p_{2x} = -\rho_2 u_2 u_{2x} - \rho_2 w_2 u_{2z}. \end{cases} \tag{A.6}$$

We rewrite the integrands in Eq. (A.2) to give

$$\begin{aligned} p_{1x} + 2\rho_1 u_1 u_{1x} &= -\rho_1 u_1 u_{1x} - \rho_1 w_1 u_{1z} + 2\rho_1 u_1 u_{1x} \\ &= \rho_1 u_1 u_{1x} - \rho_1 w_1 u_{1z}, \end{aligned} \tag{A.7}$$

$$\begin{aligned} p_{2x} + 2\rho_2 u_2 u_{2x} &= -\rho_2 u_2 u_{2x} - \rho_2 w_2 u_{2z} + 2\rho_2 u_2 u_{2x} \\ &= \rho_2 u_2 u_{2x} - \rho_2 w_2 u_{2z}. \end{aligned} \tag{A.8}$$

The mass conservation equations in the two layers are

$$\begin{cases} u_{1x} + w_{1z} = 0, \\ u_{2x} + w_{2z} = 0. \end{cases} \tag{A.9}$$

After we substitute the mass conservation equations into Eqs. (A.7) and (A.8), it yields

$$p_{1x} + 2\rho_1 u_1 u_{1x} = -\rho_1 u_1 w_{1z} - \rho_1 w_1 u_{1z}, \tag{A.10}$$

$$p_{2x} + 2\rho_2 u_2 u_{2x} = -\rho_2 u_2 w_{2z} - \rho_2 w_2 u_{2z}. \tag{A.11}$$

In order to simplify Eq. (A.2), we integral the terms in Eqs. (A.10) and (A.11) by parts, *viz.*,

$$\begin{aligned} &-\rho_1 \int_0^{\eta} w_1 u_{1z} dz - \rho_1 \int_0^{\eta} u_1 w_{1z} dz \\ &= \rho_1 \left(-u_1 w_1 |_0^{\eta} + \int_0^{\eta} u_1 w_{1z} dz \right) \\ &\quad - \rho_1 \int_0^{\eta} u_1 w_{1z} dz = -\rho_1 u_1 w_1 |_0^{\eta}, \end{aligned} \tag{A.12}$$

$$-\rho_2\int_\eta^H w_2u_{2z}dz-\rho_2\int_\eta^H u_2w_{2z}dz$$
$$=\rho_2\left(-u_2w_2|_\eta^H+\int_\eta^H u_2w_{2z}dz\right)$$
$$-\rho_2\int_\eta^H u_2w_{2z}dz=-\rho_2u_2w_2|_\eta^H. \tag{A.13}$$

Regarding the boundary condition on the top and bottom, which are

$$\begin{cases} v_1=0, & z=0;\\ v_2=0, & z=H, \end{cases} \tag{A.14}$$

Eqs. (A.12) and (A.13) can be further expanded and simplified, *viz.*,

$$-\rho_1u_1w_1|_0^\eta=-\rho_1u_1(x,\eta)w_1(x,\eta), \tag{A.15}$$

$$-\rho_2u_2w_2|_\eta^H=\rho_2u_2(x,\eta)w_2(x,\eta). \tag{A.16}$$

Eq. (A.2) can be written as

$$\frac{dS}{dx}=-\rho_1u_1(x,\eta)w_1(x,\eta)+\eta_x\rho_1u_1^2(x,\eta)$$
$$+\rho_2u_2(x,\eta)w_2(x,\eta)-\eta_x\rho_2u_2^2(x,\eta)$$
$$=\rho_1u_1(-w_1+u_1\eta_x)-\rho_2u_2(-w_2+u_2\eta_x). \tag{A.17}$$

Since the kinematical condition on the interface is

$$\begin{cases} -w_1+u_1\eta_x=0,\\ -w_2+u_2\eta_x=0, \end{cases} \tag{A.18}$$

it is concluded that

$$\frac{dS}{dx}=0, \tag{A.19}$$

which means S is a constant for any horizontal coordinate x.

Appendix B. The expansion of the stream function

Without loss of generality, only the expansion of the stream function in the lower layer is illustrated hereinafter.

The governing equation in the lower layer is

$$\Delta\Psi_1=0, \tag{B.1}$$

where Δ is Laplace operator. The boundary condition on the bottom is

$$\Psi_1|_{z=0}=C, \tag{B.2}$$

where C is a constant.

By using variables separation, the stream function can be expressed as

$$\Psi_1=\sum_{n=0}^{\infty}z^nf_n(x), \tag{B.3}$$

where f is a function with respect to the variable x. Substituting it into Eq. (B.1), we have

$$\sum_{n=0}^{\infty}z^n\left(\frac{\partial^2f_n}{\partial x^2}+(n+2)(n+1)f_{n+2}\right)=0. \tag{B.4}$$

$$\therefore\quad f_{n+2}=\frac{-1}{(n+2)(n+1)}\frac{\partial^2f_n}{\partial x^2}. \tag{B.5}$$

According to the boundary condition as shown in Eq. (B.2),

$$\because\quad \Psi_1=\sum_{n=0}^{\infty}z^nf_n(x)=C,\quad z=0. \tag{B.6}$$

$$\therefore\quad f_0=C. \tag{B.7}$$

And according to Eq. (B.5)

$$f_{2n}=0,\quad n=1,2,3,\ldots. \tag{B.8}$$

If we take C as 0, the stream function is transformed to

$$\Psi_1=\sum_{n=0}^{\infty}(-1)^n\cdot\frac{z^{2n+1}}{(2n+1)!}\cdot\frac{\partial^{2n}}{\partial x^{2n}}f_1. \tag{B.9}$$

According to its physical interpretation, f_1 in Eq. (B.9) is equivalent to $u_1(x,0)$, which is velocity on the bottom, in Eq. (15).

Appendix C. The coefficients of Eq. (52)

$$C_3=\frac{(1-\delta)\left((r-1)^2-\delta\right)}{3(r-1)((r-1)+\delta)},\quad C_4=\frac{3(1-\delta)\left((r-1)^2-\delta\right)}{2(r-1)((r-1)+\delta)},$$
$$C_5=-(1-\delta),\quad C_6=\frac{(1-\delta)\left((r-1)^2-\delta\right)}{6(r-1)((r-1)+\delta)},$$
$$C_7=\frac{(1-\delta)\left((r-1)^2-\delta\right)}{3(r-1)((r-1)+\delta)},\quad C_8=\frac{(1-\delta)\left((r-1)^2-\delta\right)}{6(r-1)((r-1)+\delta)},$$
$$C_9=\frac{(1-\delta)\left((r-1)^2-\delta\right)}{3(r-1)((r-1)+\delta)},\quad C_{10}=\frac{(1-\delta)\left((r-1)^2-\delta\right)}{6(r-1)((r-1)+\delta)},$$
$$C_{11}=\frac{(1-\delta)((r-1)^2-\delta)}{6(r-1)((r-1)+\delta)},$$
$$C_{12}=\frac{3(1-\delta)((r-1)^2-\delta)}{2(r-1)((r-1)+\delta)},$$
$$C_{13}=-\frac{1}{2}(1-\delta),C_{14}=-(1-\delta),\quad C_{15}=-\frac{1}{2}(1-\delta),$$
$$C_{16}=\frac{(1-\delta)\left((r-1)^2-\delta\right)^2\left(1-(1-r)^3\delta\right)}{45(r-1)^3((r-1)+\delta)(1+(r-1)\delta)^2},$$
$$C_{17}=\frac{(1-\delta)\left((r-1)^2-\delta\right)^2\left(1-(1-r)^3\delta\right)}{45(r-1)^3((r-1)+\delta)(1+(r-1)\delta)^2},$$
$$C_{18}=-\frac{(1-\delta)\left((r-1)^2-\delta\right)^2\left(1-(1-r)^3\delta\right)}{45(r-1)^3((r-1)+\delta)(1+(r-1)\delta)^2},$$
$$C_{19}=\frac{(1-\delta)\left((r-1)^2-\delta\right)^2\left(1-(1-r)^2\delta\right)}{45(r-1)^3((r-1)+\delta)(1+(r-1)\delta)^2},$$
$$C_{20}=-\frac{(1-\delta)\left((r-1)^2-\delta\right)^2\left(1-(1-r)^2\delta\right)}{90(r-1)^3((r-1)+\delta)(1+(r-1)\delta)^2},$$
$$C_{21}=\frac{(1-\delta)\left((r-1)^2-\delta\right)^2\left(1-(1-r)^2\delta\right)}{45(r-1)^3((r-1)+\delta)(1+(r-1)\delta)^2},$$

$$C_{22} = \frac{(1-\delta)\left((r-1)^2-\delta\right)^2\left(1-(1-r)^3\delta\right)}{45(r-1)^3((r-1)+\delta)(1+(r-1)\delta)^2},$$

$$C_{23} = -\frac{(1-\delta)\left((r-1)^2-\delta\right)^2\left(1-(1-r)^3\delta\right)}{90(r-1)^3((r-1)+\delta)(1+(r-1)\delta)^2},$$

$$C_{24} = \frac{2(1-\delta)\left((r-1)^2-\delta\right)^2\left(1-(1-r)^3\delta\right)}{45(r-1)^3((r-1)+\delta)(1+(r-1)\delta)^2},$$

$$C_{25} = -\frac{(1-\delta)\left((r-1)^2-\delta\right)^2\left(1-(1-r)^3\delta\right)}{45(r-1)^3((r-1)+\delta)(1+(r-1)\delta)^2},$$

$$C_{26} = \frac{2(1-\delta)\left((r-1)^2-\delta\right)^3\left(1-(1-r)^5\delta\right)}{945(r-1)^5((r-1)+\delta)(1+(r-1)\delta)^3},$$

$$C_{27} = -\frac{2(1-\delta)\left((r-1)^2-\delta\right)^3\left(1-(1-r)^5\delta\right)}{945(r-1)^5((r-1)+\delta)(1+(r-1)\delta)^3},$$

$$C_{28} = \frac{(1-\delta)\left((r-1)^2-\delta\right)^3\left(1-(1-r)^5\delta\right)}{945(r-1)^5((r-1)+\delta)(1+(r-1)\delta)^3},$$

$$C_{29} = \frac{(1-\delta)^2\left((1-r)^2-\delta\right)}{6(r-1)((r-1)+\delta)(1+(r-1)\delta)},$$

$$C_{30} = -\frac{(1-\delta)^2\left((1-r)^2-\delta\right)}{3(r-1)((r-1)+\delta)(1+(r-1)\delta)},$$

$$C_{31} = \frac{(1-\delta)\left((1-r)^2-\delta\right)}{6(r-1)^2(1+(r-1)\delta)},$$

$$C_{32} = \frac{(1-\delta)\left((1-r)^4-\delta\right)}{2(r-1)^3((r-1)+\delta)},$$

$$C_{33} = -\frac{(1-\delta)^2\left((1-r)^2-\delta\right)}{6(r-1)((r-1)+\delta)(1+(r-1)\delta)},$$

$$C_{34} = \frac{2(1-\delta)\left((1-r)^3-\delta\right)}{(r-1)^2((r-1)+\delta)},$$

$$C_{35} = -\frac{(1-\delta)^2\left((1-r)^2-\delta\right)}{6(r-1)((r-1)+\delta)(1+(r-1)\delta)},$$

$$C_{36} = \frac{(1-\delta)\left((1-r)^3-\delta\right)}{2(r-1)^2((r-1)+\delta)},$$

$$C_{37} = \frac{3(1-\delta)\left((1-r)^2-\delta\right)}{2(r-1)((r-1)+\delta)},$$

$$C_{38} = \frac{(1-\delta)\left((1-r)^2-\delta\right)}{2(r-1)((r-1)+\delta)}.$$

References

[1] M.H. Alford, et al., Nature 521 (7550) (2015) 65–69.
[2] Behrens, T., (2009). "OpenFOAM's basic solvers for linear systems of equations. Solvers, preconditioners, smoothers." Technical report, Technical University of Denmark, Lingby.
[3] T.B. Benjamin, J. Fluid Mech. 25 (2) (1966) 241–270.
[4] T.B. Benjamin, M. Lighthill, Proc. R. Soc. Lond. A 224 (1159) (1954) 448–460.
[5] E. Berberović, N.P. van Hinsberg, S. Jakirlić, I.V. Roisman, C. Tropea, Phys. Rev. E 79 (3) (2009) 036306.
[6] J. Boussinesq, Comp. Rend. Acad. Sci. (Paris) 72 (1871) 755–759.
[7] R. Camassa, W. Choi, H. Michallet, P.-O. Rusås, J. Sveen, J. Fluid Mech. 549 (2006) 1–23.
[8] W. Choi, R. Camassa, J. Fluid Mech. 396 (1) (1999) 1–36.
[9] J. Fenton, J. Fluid Mech. 53 (2) (1972) 257–271.
[10] F.N. Fritsch, R.E. Carlson, SIAM J. Numer. Anal. 17 (2) (1980) 238–246.
[11] J.A. Gear, R. Grimshaw, Phys. Fluids 26 (1983) 14.
[12] R. Grimshaw, J. Fluid Mech. 46 (3) (1971) 611–622.
[13] J. Grue, A. Jensen, P.-O. Rusås, J.K. Sveen, J. Fluid Mech. 380 (1999) 257–278.
[14] A. Harten, J. Comput. Phys. 49 (3) (1983) 357–393.
[15] P. Higuera, J.L. Lara, I.J. Losada, Coast. Eng. 71 (0) (2013) 102–118.
[16] W.-H. Huang, Y.-X. You, X. Wang, T.-Q. Hu, Acta Phys. Sin. 62 (8) (2013) 084705.
[17] R.I. Issa, J. Comput. Phys. 62 (1) (1986) 40–65.
[18] N.G. Jacobsen, D.R. Fuhrman, J. Fredsøe, Int. J. Numer. Meth. Fluids 70 (9) (2012) 1073–1088.
[19] Jasak, H., (1996). "Error analysis and estimation for the finite volume method with applications to fluid flows," PhD thesis, Department of Mechanical Engineering, Imperial College of Science, Technology and Medicine.
[20] T. Kakutani, N. Yamasaki, J. Phys. Soc. Jpn. 45 (2) (1978) 674–679.
[21] G.H. Keulegan, J. Res. Natl. Bureau Standards 51 (1953) 133–140.
[22] C.G. Koop, G. Butler, J. Fluid Mech. 112 (1981) 225–251.
[23] D.J. Korteweg, G. De Vries, Lond. Edinb. Dublin Philos. Mag. J. Sci. 39 (240) (1895) 422–443.
[24] D. Kothe, W. Rider, S. Mosso, J. Brock, J. Hochstein, AIAA Pap. 96 (0859) (1996) 1–18.
[25] E. Kreyszig, Advanced Engineering Mathematics, Wiley, 2011.
[26] E. Laitone, J. Fluid Mech. 9 (03) (1960) 430–444.
[27] M.J. Lighthill, Philos. Mag. 40 (311) (1949) 1179–1201.
[28] A.K. Liu, Y.S. Chang, M.K. Hsu, N.K. Liang, J. Geophys. Res: Oceans 103 (C4) (1998) 7995–8008.
[29] R.R. Long, Tellus 8 (4) (1956) 460–471.
[30] R.M. Mirie, S.A. Pennell, Phys. Fluids A 1 (6) (1989) 986–991.
[31] R.M. Mirie, C. Su, J. Fluid Mech. 147 (1) (1984) 213–231.
[32] W.F. Noh, P. Woodward, in: Proceedings of the Fifth International Conference on Numerical Methods in Fluid Dynamics, Enschede . Springer, Twente University, 1976, pp. 330–340.
[33] OpenFOAM documentation, OpenFOAM User Guide, OpenFOAM Foundation, (2014).
[34] A.R. Osborne, T.L. Burch, Science 208 (4443) (1980) 451–460.
[35] L. Ostrovsky, Y.A. Stepanyants, Rev. Geophys. 27 (3) (1989) 293–310.
[36] L.A. Ostrovsky, J. Grue, Phys. Fluids 15 (2003) 2934.
[37] S. Patankar, Numerical Heat Transfer and Fluid Flow, CRC Press, 1980.
[38] Rusche, H., (2002). "Computational fluid dynamics of dispersed two-phase flows at high phase fractions," PhD thesis, Imperial College London (University of London).
[39] T. Stanton, L. Ostrovsky, Geophys. Res. Lett. 25 (14) (1998) 2695–2698.
[40] Ubbink, O., (1997). "Numerical prediction of two fluid systems with sharp interfaces," PhD thesis, University of London, UK.
[41] B. van Leer, J. Comput. Phys. 135 (2) (1997) 229–248.
[42] H.G. Weller, G. Tabor, H. Jasak, C. Fureby, Comput. Phys. 12 (6) (1998) 620–631.
[43] P. Wesseling, Principles of Computational Fluid Dynamics, Springer Science & Business Media, 2009.